

# Effect of reversion of strain induced martensite on microstructure and mechanical properties in an austenitic stainless steel

S. K. Ghosh · P. Mallick · P. P. Chattopadhyay

Received: 27 November 2010 / Accepted: 6 January 2011 / Published online: 19 January 2011  
© Springer Science+Business Media, LLC 2011

**Abstract** Effect of reversion of strain induced  $\alpha'$  martensite on mechanical properties of an austenitic stainless steel has been examined. The  $\alpha'$  martensite formed by cold rolling (40%) at 0 °C has been reverted to austenite by carrying out annealing in the temperature range of 300–800 °C for 1 h. Microstructural investigation has demonstrated the enhanced reversion with increasing annealing temperature without any perceptible grain growth up to 800 °C. X-ray diffraction (XRD) analysis has revealed that 40% cold rolling has resulted in the formation of 32% martensite. The residual martensite content has been found to be about 8% after reversion at 800 °C. Different stages of reversion behavior has been examined by differential scanning calorimetric measurement. The variation of  $d\sigma/d\varepsilon$  with  $\varepsilon$  is examined to identify different stages of work hardening of the investigated steel. Both tensile strength and percent elongation values increase with increasing annealing temperature up to 500 °C. Beyond that annealing treatment results in the drop of tensile strength value with the consequent increase in percent elongation. Attractive strength–ductility combination (22.80 GPa%) has been achieved after annealing of the 40% cold deformed specimen at 800 °C for 1 h. The fractographic observation corroborates the tensile results.

## Introduction

Austenite in steel exhibits deformation induced transformation into martensite within the temperature range marked by  $M_S$  and  $M_{d30}$  as the lower and upper limits, respectively, following the sequence of  $\gamma$ (FCC)  $\rightarrow \varepsilon$  (HCP)  $\rightarrow \alpha'$ (BCC) transformation [1, 2]. The amount of  $\alpha'$  martensite depends on the deformation methods, amount of plastic strain, strain rate, and temperature [3–5]. Stacking fault energy (SFE) of austenite which is a function of temperature and composition governs the dominant deformation mechanism. For higher SFE ( $>20$  mJ/m<sup>2</sup>) the deformation mode is shifted from  $\varepsilon$  martensite formation to deformation twining and then slip [6]. Plastic deformation of the austenite creates the proper defect structure which acts as the embryo for the transformation product. In austenitic stainless steels, embryos are formed at the intersections of shear bands, e.g., stacking faults, twins, etc. [4, 7, 8]. Usually  $\varepsilon$  martensite is formed at the low deformation level (i.e., 5–10%) and at the higher strain levels, the  $\alpha'$  martensite increases at the expense of  $\varepsilon$  martensite [9]. The morphology of the transformation product is typically lath-like [1, 4]. In respect of the effect of composition, at considerably lower temperatures,  $\delta$ -ferrite forming elements like, Cr, Si, Mo act as strong austenite stabilizer in the same way as Ni, Mn, C, N, etc. The upper limit of the transformation temperature is obtained as [3]:

$$M_{d30}(\text{°C}) = 413 - 462(C + N) - 9.2(Si) - 8.1(Mn) - 13.7(Cr) - 9.5(Ni) - 18.5(Mo) \quad (1)$$

where elements are in wt%.

Reversion of strain induced martensite to austenite (e.g.,  $\alpha' \rightarrow \gamma$ ) improves mechanical properties by grain refinement [10, 11] which is known to improve the both strength and toughness of structural steels. Grain refinement

S. K. Ghosh (✉) · P. Mallick · P. P. Chattopadhyay  
Department of Metallurgy and Materials Engineering,  
Bengal Engineering and Science University, Shibpur,  
Howrah 711103, India  
e-mail: skghosh@metal.becs.ac.in

processes are greatly influenced by the reversion mechanism [12]. There are two types of mechanism for the reversion from martensite to austenite: one is diffusional reversion and the other is martensitic shear reversion without diffusional process. The steels which undergo martensitic shear reversion, reversion completes during heating and reverse austenite contains a high density of dislocations just after reversion. It has been found that, increase in Ni/Cr ratio lowers the martensitic shear reversion temperature by increasing the Gibbs free energy change between FCC and BCC structure [12]. Steels with high Ni/Cr ratio (0.625) easily undergo the martensitic reversion in a low temperature range. During successive annealing, grain refinement proceeds through the process of recrystallization of reverse austenite. Defects such as dislocations and slip bands were inherited to reversed austenite resulting to grain refinement. On the other hand, diffusional reversion proceeds by the growth of austenite nucleated in the martensite lath boundary which contains high dislocation density.

Austenitic steels do not undergo phase transformation at typical annealing temperatures and the only way to refine the grain is recrystallization after cold rolling. However, the strengthening by grain refinement is limited due to the high recrystallization temperature ( $>900$  °C) of this stainless steel grade. In austenitic stainless steels, plastic deformation of austenite creates the proper defect structures which act as embryo for martensite transformation which reverts to recrystallized austenite during annealing in the temperature range of 450–800 °C [13–15]. Therefore, it is of interest to consider the effectiveness of reversion as a means of strengthening steels. The strengthening effect in the austenite depends in a complex manner on many factors relating to alloy constitution, structure, and heat treatment conditions. The increase in strength of austenite achieved by reversion is associated with the high dislocation density of the reversed austenite regions and the presence of stacking faults and twins.

In view of the above, the present work aims to examine the effect of reverse transformation of strain induced martensite on microstructure evolution as well as mechanical properties after annealing over the temperature range of 300–800 °C for 1 h duration. The process of reversion including recovery and precipitation has been examined by calorimetric measurements.

## Experimental

The austenitic stainless steel has been considered for this study. Result of the spectroscopic analysis conducted by using an Optical Emission Spectrometer (ARL 4460) is shown in Table 1. The as received hot rolled steel plates

**Table 1** Chemical composition of the investigated stainless steel (wt%)

C	Mn	Si	S	P	Cr	Ni	Fe
0.08	1.51	0.76	0.017	0.030	18.94	8.56	Bal.

(~20 mm thick) were cold rolled (40%) at 0 °C. Since it has earlier been reported that substantial amount of martensite is achieved beyond 20% deformation [12], it was considered appropriate to carry out the study with one particular reduction, i.e., 40% to assess the role of reversion process. The deformed samples were subjected to inter-pass cooling in ice-water mixture to avoid the effect of adiabatic heating during rolling.

Samples with the dimensions of 15 × 10 × 6 mm<sup>3</sup> were cut from the cold deformed plate for annealing treatments. The annealing treatments were conducted in a Muffle furnace at different temperatures ranging from 300 to 800 °C with the intervals of 100 °C for 1 h duration.

Samples prepared by following standard metallographic technique were etched using aqua regia solution (75% HCl and 25% HNO<sub>3</sub> mixture). Properly etched samples were examined at appropriate magnifications using a scanning electron microscope (SEM) (Model: JEOL, JSM-5510) operated at a 15–20 kV. Energy dispersive X-ray spectroscopic analysis (EDS) was conducted to determine the chemical composition of precipitate phases. The tensile fracture surfaces as well as sub-surfaces close to the fracture surfaces were also studied under SEM.

Small rectangular specimen (15 × 12 × 3 mm<sup>3</sup>) was mechanically polished followed by chemically polishing, using a mixture of hydrochloric acid, nitric acid and distilled water in 1:1:1 proportion, to remove the residual stress in the surface. The X-ray diffraction (XRD) study of the samples was conducted by using a Philips diffractometer (PW 1710) with Cu K<sub>α</sub> radiation with 40 kV operating voltage, 30 mA current and 0.003° 2θ s<sup>-1</sup> scan rate. Quantitative estimation of the phases (austenite and martensite) was performed by Rietveld analysis [16] of the X-ray data using commercial software, X'Pert High Score Plus.

Differential scanning calorimetry (DSC) studies of some selected deformed samples (~15 mg) were carried out using METTLER TA 4000 system using high purity argon atmosphere. Heating runs were carried out at heating rates ( $\phi$ ) of 5, 10, and 20 °C/min up to a temperature of 700 °C which was identified as almost the saturation temperature for the reversion transformation.

A Brinell-cum-Vickers hardness tester (Model: BV-250 (SPL)) was used to measure the Vickers hardness values of the cold deformed samples as well as to assess the reversion effect under 30 kg load. At least six indentations were

taken on each sample (on rolling plane) and the average hardness value was reported.

Room temperature tensile testing was carried out using a computer controlled Instron-4204 testing machine with a crosshead velocity of 0.5 mm/min. The test specimen was prepared as per ASTM Standard (ASTM: Vol. 03.01, E8M-96). The yield strength (YS), ultimate tensile strength (UTS), and percent total elongation (%TEL) was determined from the machine output.

## Results and discussion

### Microstructure

Figure 1a and b shows the SEM micrographs obtained from the as received sample and after subjecting the same to 40% cold deformation. The as received specimen (Fig. 1a) reveals fully austenitic structure ( $\sim 23 \mu\text{m}$ ) and presence of annealing twins therein.

Generally the microstructure of the cold rolled steel is characterized by the dispersion of hard martensite in a deformed austenite matrix. In this context, the SFE for the present steel has been estimated as  $18 \text{ mJ/m}^2$  using the following equation [17]

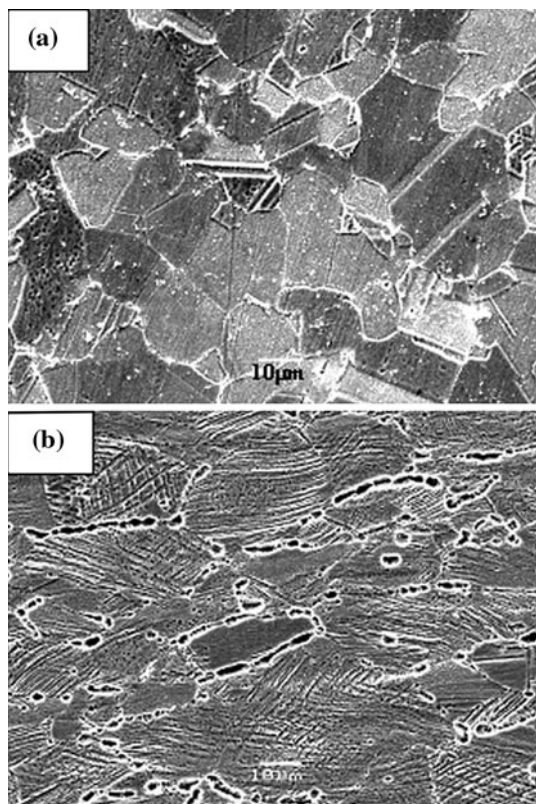


**Fig. 1** SEM micrograph of investigated stainless steel in **a** as received condition and **b** cold deformed (40%) condition

$$\begin{aligned} \text{SFE}(\text{mJ/m}^2) = & -53 + 6.2(\text{Ni}) + 0.7(\text{Cr}) \\ & + 3.2(\text{Mn}) + 9.3(\text{Mo})(\text{wt}\%) \end{aligned} \quad (2)$$

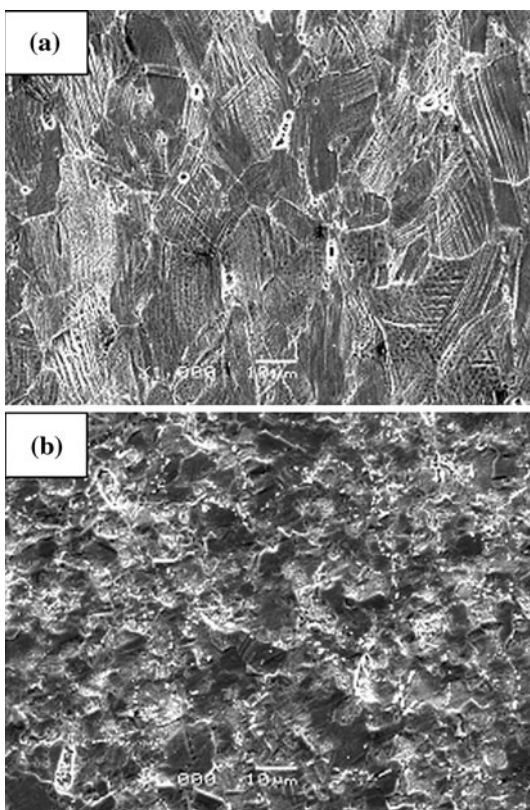
Such SFE value is favorable for the formation of microtwins and hence the formation of  $\alpha'$  becomes easier. In this study, deformation with 40% reduction results into the austenite grains elongated along the rolling direction and the formation of strain induced  $\alpha'$  (Fig. 1b) at the intersections of microtwins during deformation. Earlier, small amount of  $\alpha'$  has been achieved for as low as 16% cold [18] deformation. The diffused nature [19] of austenite grains is apparently the manifestation of severe deformation. The deformation induced martensite (DIM) morphology is narrower and more elongated than the thermally induced martensite [20]. The dislocation substructures are created within the martensite due to accommodation of plastic deformation associated with the transformation. Formation of the high density of dislocation and the dislocation–precipitate interaction in  $\alpha'$  martensite in the similar austenitic steel after deformation has been elegantly demonstrated in the earlier studies [18, 19]. The micrograph (Fig. 1b) further reveals the intergranular microcracking at some locations. This is attributed to the accommodation strain during 40% cold reduction.

Figure 2a reveals that after annealing treatment at  $500^\circ\text{C}$  for 1 h, the DIM undergoes reversion (i.e.,  $\alpha' \rightarrow \gamma$ ) along the martensite/austenite interface as a result of thermal decomposition of strain induced martensite. The reverted austenite grows at the expense of strain induced  $\alpha'$  martensite. It is apparent that individual  $\alpha'$  martensite phase breaks up during reversion, while the other areas of the specimen appear to be unaffected by the heating. It is important to mention that the intergranular microcracking has been significantly reduced after annealing due to the release of the residual stress of 40% cold deformed sample.

Figure 2b demonstrates that the reversion rate increases with the progress of annealing. The mechanism initiates with reversion of strain induced martensite to austenite through diffusion or shear mechanism. Then the newly formed austenite undergoes recovery and recrystallization. This leads to the formation of finer ( $10\text{--}15 \mu\text{m}$ ) strain free equiaxed austenite grain. The micrograph also reveals the formation of fine precipitates of brighter contrast along the austenite grain boundary and twin boundaries. The average chemical composition of the brighter precipitate particles obtained from EDS microanalysis is  $68.63\text{Fe}-22.50\text{Cr}-7.41\text{Ni}-0.52\text{Si}-0.94\text{Mn}$  (wt%) which indicates the formation of  $(\text{Cr}, \text{Fe})_{23}\text{C}_6$  phase [21].

### XRD

Figure 3 shows the XRD profiles of the cold deformed samples after annealing at different temperatures in the



**Fig. 2** SEM micrograph of 40% cold deformed stainless steel specimen subjected to annealing for 1 h at **a** 500 °C and **b** 800 °C

range of 300–800 °C for 1 h duration. The XRD plot of the ‘as-received’ specimen (0% deformation) has also been appended to reveal the peaks related to the single phase austenite. In the case of the deformed sample, the (110), (200), and (211) peaks of the BCC  $\alpha'$  martensite phase are clearly revealed along with the (111), (200), (220), (311), and (222) peaks characterizing the FCC austenite phase. However, the XRD pattern does not reveal any peak related to  $\varepsilon$  martensite. In this context, it is known that crystal structure of  $\varepsilon$  martensite is heavily faulted [22, 23] due to overlapping stacking faults resulting in low intensity and increased width of the concerned XRD peaks.

In this study, quantitative estimation of phases from the XRD pattern of the cold deformed sample has yielded 32% strain induced  $\alpha'$  martensite. It has earlier been reported that the quantification of  $\alpha'$  martensite by XRD is not reliable below 15% reduction [19]. It is also noteworthy that  $M_{d30}$  temperature of the present steel has been found to be around 16° from the empirical equation proposed by Angel [3]. Hence, 40% cold rolling at 0 °C was considered to be conducive for the formation of stain induced martensite.

The annealing treatment in the temperature range of 300–800 °C for 1 h duration resulted into the reversion of strain induced martensite. An increase in the annealing

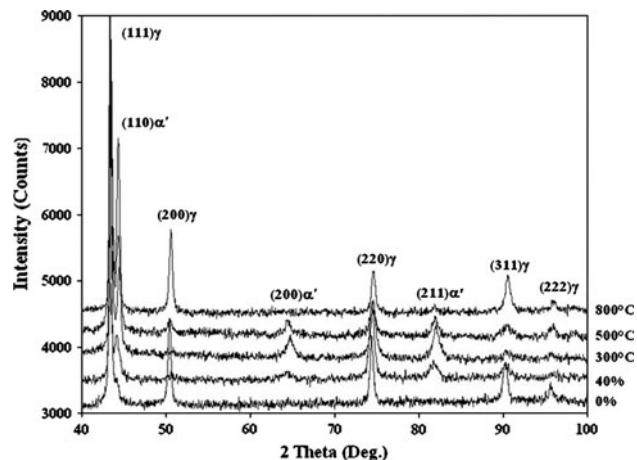


**Fig. 3** XRD patterns depicting the formation of strain induced martensite ( $\alpha'$ ) by cold deformation and its reversion into austenite ( $\alpha' \rightarrow \gamma$ ) after annealing (300–800 °C, 1 h)

temperature from 300 to 800 °C evidences more prominent  $\alpha' \rightarrow \gamma$  transformation. It is also apparent that the peaks related to the  $\alpha'$  martensite become weaker or disappear after the annealing treatments. Earlier, Rathbun et al. [24] have reported that volume fraction of  $\alpha'$  martensite does not change significantly during low temperature ageing (300 °C) and phase transformation occurs when the temperature exceeds 450 °C. This is in agreement to the aforesaid results. The measured residual volume percent of strain induced  $\alpha'$  martensite after annealing at 800 °C for 1 h is 8%.

In this study, the peak related to Cr-carbide has not appeared in the XRD patterns. It implies that the volume percent of Cr-carbide is inadequate for estimation by the XRD.

#### DSC study

In this study, kinetics of different processes associated with annealing of the cold rolled stainless steel has been studied by DSC technique. Figure 4 shows the DSC thermograms obtained from the 40% deformed sample at the heating rate of 5, 10, and 20 °C/min, respectively. For all the heating rates, the plots reveal one endothermic peak in the temperature range of 300–400 °C and two exothermic peaks in the temperature range of 400–550 °C and 600–700 °C. For the heating rates of 5 and 10 °C/min, additional exothermic peaks appear at 270 and 318 °C which concern segregation and clustering of carbon atoms [25]. At higher heating rate (20 °C/min), the heat release associated with these exothermic peak overlaps with the heat absorption associated with the subsequent transformation and do not appear distinctly in the thermogram.

Earlier, it has been identified that the endothermic peak between 300 and 400 °C is due to the dissolution of

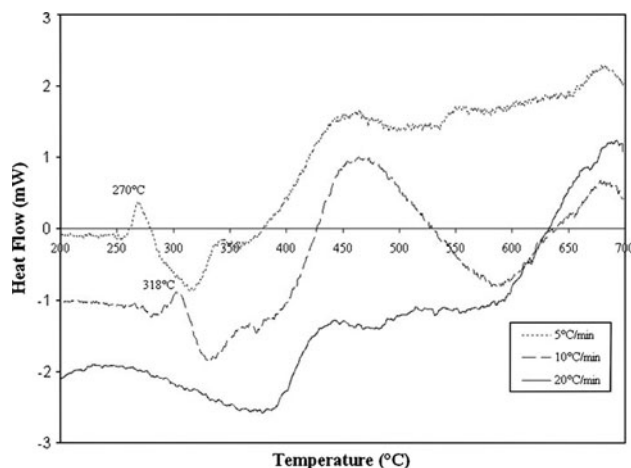


**Fig. 4** DSC plots obtained at 5, 10, and 20 °C/min for the samples subjected to 40% cold deformation

martensite and crystal defect occurring at the initial stage of the reverse transformation of DIM in small regions along the austenite/martensite interface [26]. Simultaneous diffusion of Fe and Ni across the austenite/martensite interface seems to stabilize the rest of martensite by interrupting the reverse transformation in the temperature range of 400–450 °C. The exothermic peak in the temperature range of 400 and 550 °C might be related to one or more microstructural evolutions such as recovery of  $\alpha'$  martensite, the precipitation of carbides or the additional formation of  $\alpha'$  martensite [18]. The prominent exothermic

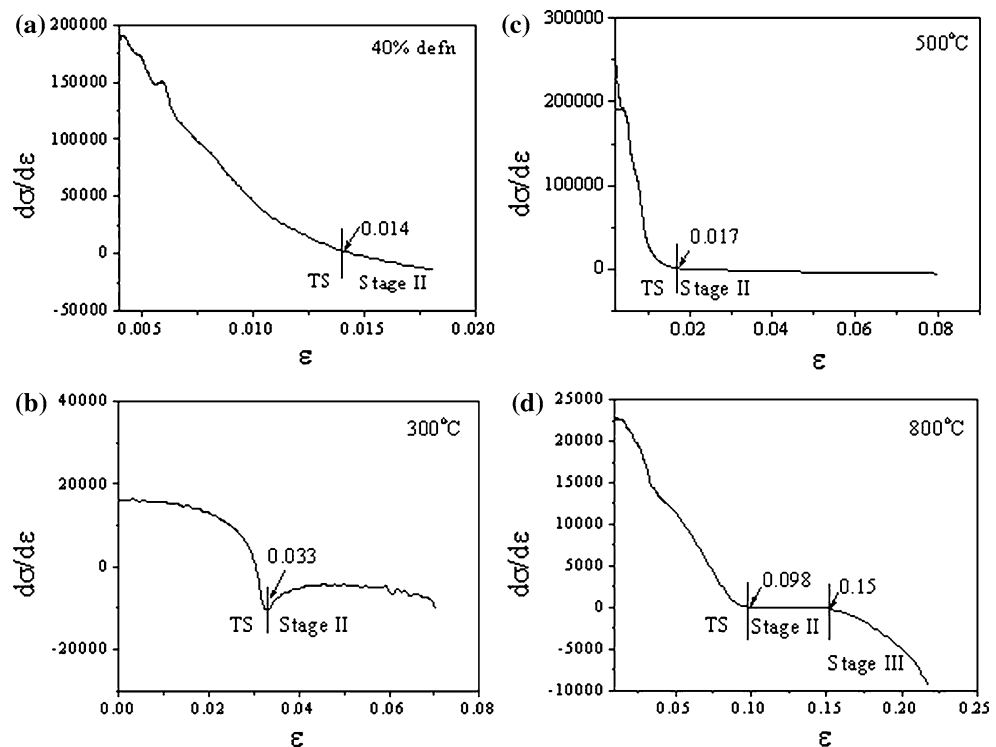
peak between 600 and 700 °C indicate the precipitation of chromium carbide. Although, the temperature of  $\sim 600$  °C is apparently low for the precipitation of  $(\text{Cr}, \text{Fe})_{23}\text{C}_6$  [21], the prior cold deformation supports the same in the present case.

#### Work hardening behavior

The variation of  $d\sigma/d\varepsilon (\theta)$  with  $\varepsilon$  is widely used to interpret tensile work hardening behavior [27, 28]; thereby attempted to examine the different stages of work hardening of the investigated steel. The plots of  $\theta$  versus  $\varepsilon$  at a strain rate of  $3.3 \times 10^{-4} \text{ s}^{-1}$  are presented in Fig. 5a–d for cold deformed (40%) specimen along with those annealed at low (300 °C), intermediate (500 °C), and high (800 °C) temperatures, respectively. All the plots exhibit an initial transient stage (TS) of rapid decrease in  $\theta$  (stage I) followed by a region of plateau or gradual decrease (stage II). However, Fig. 5d shows the three-stage behavior, whereas  $\theta$  decreases with  $\varepsilon$  due to onset of dynamic recovery in stage III. It can be mentioned that while the stage II is more pronounced at intermediate temperature, stage III is evident at higher annealing temperature (800 °C). It is noteworthy that these observations are in accordance with the results of similar steels reported earlier [29, 30].

In the TS (stage I), dislocation velocity, and mobile dislocation density increases which lead to rapid increase in plastic strain rate immediate after elastic limit [31]. This stage is attributed to the stabilization of the plastic strain

**Fig. 5** Variation in strain hardening rate ( $d\sigma/d\varepsilon$ ) as a function of true strain ( $\varepsilon$ ) at **a** 40% cold deformed sample, **b** 300 °C, **c** 500 °C, and **d** 800 °C



rate with the dislocation source density. In this study, the low value of SFE (i.e., 18 mJ/m<sup>2</sup>) prevents the cross-slip of dislocations at low strain which results the occurrence of stage I. While the transition from stage I to stage II at 300 °C occurs at the 3.3% strain, the same is found to be as lower values (1.7%) for 500 °C. The higher value of transition strain (9.8 and 15% for stage II and stage III) obtained after annealing at 800 °C can be attributed to the coarse grain size of steel. The rapid increase in dislocation density in stage II with plastic strain signifies the characteristic feature (i.e., storage of dislocation) [29] of stage II hardening.

In Fig. 5d, the dominant recovery in stage III is noticeable as a decrease in  $\theta$  with respect to  $\varepsilon$  with increasing temperature. The increased rate of dynamic recovery is attributed to early cross-slip and climb of dislocations. The rapid increase of the sub-grain size above 0.5T<sub>m</sub> due to dynamic recovery [32, 33] leads to the observed decrease in  $\theta$ .

#### Mechanical properties

Figure 6 shows the effect of annealing temperature on hardness, yield strength, ultimate tensile strength, and percent elongation of the cold rolled (40%) specimens annealed for 1 h. The hardness value of the as received sample is 215 VHN, which reaches to 392 VHN after 40% cold reduction. The high level of hardness value is attributed to the transformation of austenite to  $\alpha'$  martensite. The hardness, yield, and tensile strength of cold deformed specimen increase continuously with annealing temperature up to 400 °C and then decrease rapidly. The increment of hardness, yield and tensile strength values are 13 HV, 46 MPa, and 75 MPa, respectively, at the peak temperature as compared with those of the cold rolled steel. In this

context, it may be mentioned that the XRD result reveals the presence of 32% strain induced  $\alpha'$  martensite in cold deformed sample. XRD result (Fig. 3) further indicates higher amount of (>32%)  $\alpha'$  martensite for an annealed sample at 400 °C which is in agreement to the earlier results [18]. The increment of hardness and strength is closely related to the variation of the amount of dislocation density and strain induced  $\alpha'$  martensite with annealing temperature.

Generally, a cold rolled stainless steel is characterized by the increase of strength with consequent lowering of percent elongation. The yield strength has been significantly increased to 1250 MPa, which is more than 4.5 times higher than that of the as received sample (271 MPa). 40% cold reduction also increases the tensile strength in two times of magnitude, i.e., from 710 MPa (as received) to 1444 MPa with the drastic reduction of percent elongation from 57% (as received) to 2%. The improvement of strength and drop in elongation by cold deformation is attributed to the strain induced  $\alpha'$  martensite in addition to the strain hardening of high alloyed austenite [34]. It is important to note that during the course of annealing both tensile strength and percent elongation increase. Usually an increment of tensile strength results in the decrease of percent elongation. Earlier, it has been reported that increase in tensile strength and percent elongation in similar steel corresponds with the reduction in void nucleation site during the tensile test [35, 36]. In this study, annealing in the temperature range of 300–400 °C reduces the void nucleation site during tensile test; both the tensile strength and percent elongation might increase. The strength value drops down to 1046 MPa with the 13% increase of percent elongation after annealing at 800 °C. The hardness value of 222 VHN is obtained which is approximately equal to the hardness value of the as received specimen. This combination of mechanical property is attributed to the annihilation of dislocation density, formation of finer (10–15 μm) strain free reverted austenite grain along with the fine precipitates of (Cr, Fe)<sub>23</sub>C<sub>6</sub> phase as depicted in Fig. 2b.

#### Fracture surface and sub-surface

To understand the micromechanism of fracture, tensile fracture surfaces as well as sub-surfaces just underneath the fracture surfaces have been studied using SEM. The tensile fracture surface of as received specimen (Fig. 7a) reveals predominantly ductile fracture with varying dimple size and depths. The size of the dimple is extremely fine which indicates higher ductility (57%). Sub-surface micrograph (Fig. 7b) reveals the frequent nucleation of micro-voids at the austenite/martensite interface as well as nucleation and propagation of microcracks within the martensite (denoted by white arrow). Formation of microcracks by fracturing

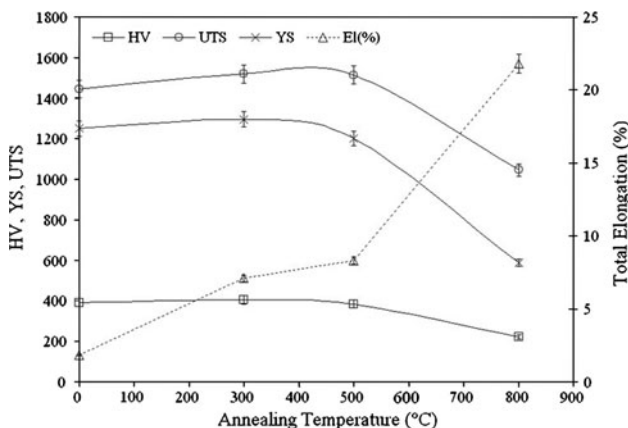


**Fig. 6** Variation of hardness, yield strength, ultimate tensile strength, and percent elongation with the annealing temperature (time = 1 h)

martensite phase (marked by black arrow in Fig. 7b) is also evident.

The fractograph of deformed and annealed ( $300\text{ }^{\circ}\text{C}$ , 1 h) specimen as shown in Fig. 7c shows the typical quasi-brittle nature. The fractographic features of the sample are in conformance with the corresponding percent elongation values. The sub-surface micrograph (Fig. 7d) clearly indicates that the microvoids are essentially nucleated along the austenite/martensite and/or martensite/martensite interface which results the rapid void coalescence and tensile fracture becomes predominantly intergranular in nature. The microvoids are elongated toward the tensile loading direction for as received specimen, while the same appears to be nearly spherical (denoted by white arrow) for cold rolled and annealed ( $300\text{ }^{\circ}\text{C}$ ) specimen (Fig. 7b vis-à-vis Fig. 7d) indicating less ductility in the latter one.

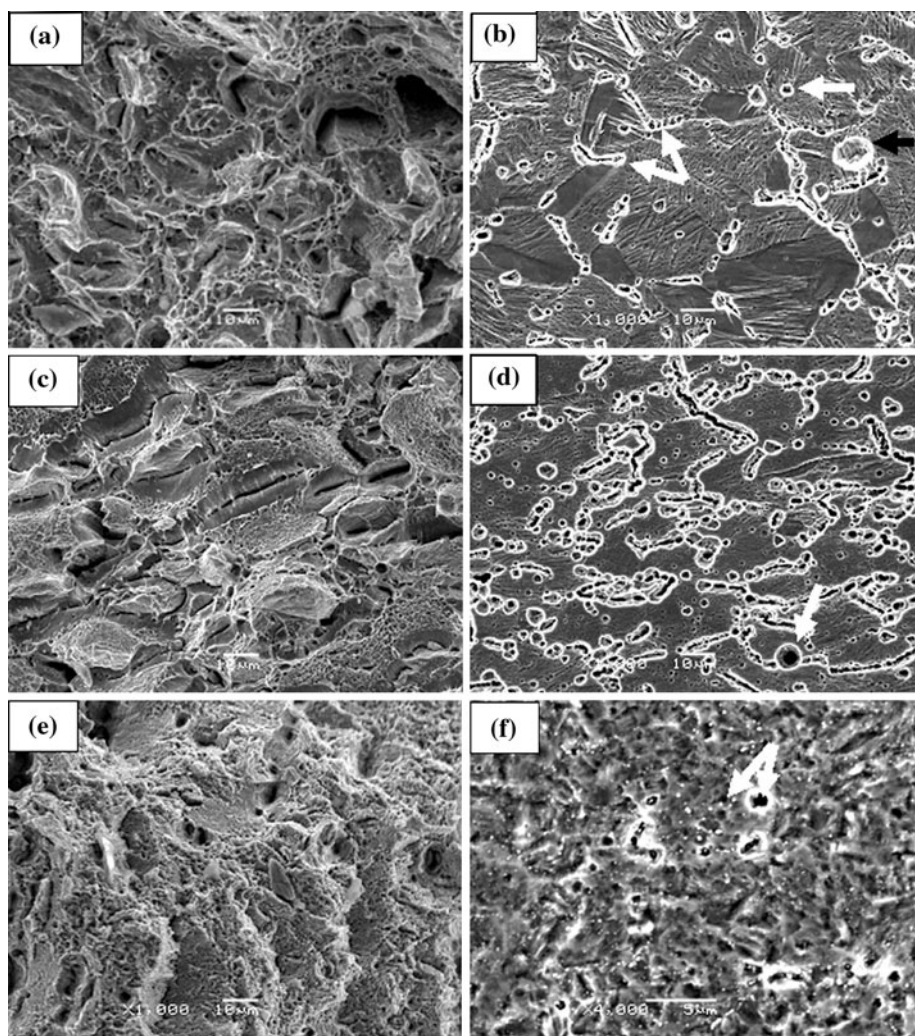
The fractograph of deformed and annealed ( $800\text{ }^{\circ}\text{C}$ , 1 h) specimen as shown in Fig. 7e shows the quasi-brittle nature. The sub-surface micrograph (Fig. 7f) demonstrates

that the voids are nucleated from the austenite/martensite interface as well as from the precipitate particle/austenite phase interface (denoted by white arrow). The quasi-brittle fracture behavior may be attributed to the presence of chromium rich carbide phase in austenite which offers some resistance to the motion of advancing crack. The fine recrystallized reverted austenite grains (Fig. 2b) are favorable for increased plasticity. As a consequence, the sample reveals higher percent elongation as compared to that of the former one (Fig. 7c).

## Conclusions

1. Microstructural examination has demonstrated that the reversion transformation has enhanced with increasing annealing temperature but no grain growth is observed up to  $800\text{ }^{\circ}\text{C}$ . Cr-carbide precipitation at austenite grain boundaries is prominent at higher annealing temperature ( $800\text{ }^{\circ}\text{C}$ ).

**Fig. 7** SEM photographs of **a** tensile fracture surface of as received specimen; **b** microstructure of sub-surface close to the fracture surface; **c** fracture surface of deformed and annealed ( $300\text{ }^{\circ}\text{C}$ , 1 h) specimen; **d** microstructure of sub-surface; **e** fracture surface of deformed and annealed ( $800\text{ }^{\circ}\text{C}$ , 1 h) specimen; and **f** microstructure of sub-surface. Arrows in **b**, **d**, and **f** indicate the sites of cracks and/or void nucleation



2. XRD analysis has revealed that the 40% cold deformation at 0 °C results in the formation of 32% strain induced  $\alpha'$  martensite as well as its reversion into austenite after annealing (300–800 °C, 1 h). The measured residual volume percent of  $\alpha'$  martensite after annealing at 800 °C for 1 h is 8%.
3. Temperatures concerning the different stages of the reversion process including the Cr-carbide precipitation have been identified by differential calorimetric measurement.
4. The variation of  $d\sigma/d\varepsilon$  with  $\varepsilon$  is used to examine the different stages of work hardening of the investigated steel. Both tensile strength and percent elongation values increase with increasing annealing temperature up to 450 °C beyond that annealing result in drop of tensile strength value with the consequent rise in percent elongation. 40% cold deformation and annealing at 800 °C for 1 h has resulted into attractive strength–ductility combination (22.80 GPa%).
5. The fractographic observation corroborates the results obtained from the tensile testing. The sub-surface micrographs provide the potential sites for the initiation of microvoids and/or microcracks.

## References

1. Olson GB, Cohen M (1972) J Less Common Metals 28:107
2. Maxwell PC, Goldberg A, Shyne JC (1974) Metall Trans 5:1305
3. Angel T (1954) J Iron Steel Inst 177:165
4. Manogonon PL, Thomas G (1970) Metall Trans 1A:1577
5. Huang GL, Matlock DK, Krauss G (1989) Metall Mater Trans 20A:1239
6. Chio JY, Jin W (1997) Scr Mater 36:99
7. Venables JA (1962) Philos Mag 7:35
8. Lagneborg R (1964) Acta Met 12:823
9. Manogonon PL, Thomas G (1970) Metall Trans 1A:1587
10. Ono K, Koppenaal TJ (1974) Metall Trans 5:739
11. Tokizane M, Matsumura N, Tsuzaki K, Maki T, Tamura I (1982) Metall Trans A 13A:1379
12. Tomimura K, Takaki S, Tokunaga Y (1991) ISIJ Int 31:1431
13. Di Schino A, Barteri M, Kenny JM (2002) J Mater Sci Lett 21:751
14. Smith H, West DRF (1973) J Mater Sci 8:1413. doi: [10.1007/BF00551664](https://doi.org/10.1007/BF00551664)
15. Johannsen DL, Kryolainen A, Ferreira PJ (2006) Metall Trans 37A:2325
16. Hill RJ, Howard CJ (1987) J Appl Cryst 20:467
17. Schramm RE, Reed RP (1974) Metall Trans 6:1345
18. Lee SH, Lee JC, Choi JY, Nam WJ (2010) Met Mater Int 16:21
19. Mumtaz K, Takahashi S, Echigoya J, Kamada Y, Zhang LF, Kikuchi H, Ara K, Sato M (2004) J Mater Sci 39:85. doi: [10.1023/B:JMSC.0000007731.38154.e1](https://doi.org/10.1023/B:JMSC.0000007731.38154.e1)
20. Güner M, Güler E, Aktas H (2008) Mater Charact 59:498
21. Padilha AF, Rios PR (2002) ISIJ Int 42:325
22. Bowkett MW, Keown SR, Harries DR (1982) Met Sci 16:499
23. Fujita H, Ueda S (1972) Acta Metall 20:759
24. Rathbun RW, Matlock DK, Krauss G (2000) Scr Mater 42:887
25. Morra PV, Böttger AJ, Mittemeijer EJ (2001) J Therm Anal Calorim 64:905
26. Kessler H, Pitsch W (1967) Acta Metall 15:401
27. Kocks UF (1976) J Eng Mater Technol 98:76
28. Estrin Y, Mecking H (1984) Acta Metall 32:57
29. Feaugas X (1999) Acta Metall 47:3617
30. Isaac Samuel E, Choudhary BK, Bhanu Sankara Rao K (2002) Scr Mater 46:507
31. Ray SK, Samuel KG, Rodriguez P (1992) Trans Indian Inst Met 45:257
32. Michel DJ, Motteff J, Lovell AJ (1973) Acta Metall 21:1269
33. Kashyap BP, McTaggart K, Tangri K (1988) Philos Mag 57:97
34. Soman MC, Juntunen P, Karjalainen LP, Misra RDK, Kyrolainen A (2009) Metall Trans A 40A:729
35. Nan HN, Lee CG, Suh DW, Kim SJ (2008) Mater Sci Eng A 485:224
36. Nan HN, Oh CS, Kim G, Kwon O (2009) Mater Sci Eng A 499:462